Mass spectra and decay properties of the higher excited ρ mesons

Xue-Chao Feng,[1] Zheng-Ya Li,[2] De-Min Li,[2,*] Qin-Tao Song,[2,†] En Wang,[2,‡] and Wen-Cheng Yan[2,§]

[1]*College of Physics and Electronic Engineering, Zhengzhou University of Light Industry, Zhengzhou 450002, China*

[2]*School of Physics and Microelectronics, Zhengzhou University, Zhengzhou, Henan 450001, China*

(Received 23 June 2022; accepted 10 October 2022; published 24 October 2022)

Although there are some experimental hints for the higher excited ρ mesons, our knowledge of their properties is theoretically very poor. Based on our recent work about excited ρ mesons [Z. Y. Li *et al.*, Phys. Rev. D **104**, 034013 (2021)], we present the mass spectra and decay properties of the higher excited ρ mesons with the modified Godfrey-Isgur quark model and the $^3P_0$ strong decay model, and compare our predictions with the experimental hints, which should be helpful to search for these higher excited ρ mesons.

DOI: 10.1103/PhysRevD.106.076012

I. INTRODUCTION

In the last decades, a large number of light vector mesons with masses below 2.4 GeV have been reported experimentally [1–7], and a lot of research has been conducted theoretically based on these experimental data [8–15]. These experimental and theoretical studies are crucial to deepen our understanding of the light vector mesons. In addition, the higher excited light vector mesons above 2.4 GeV play an important role in the processes involving the baryon antibaryon interactions [16]. However, there are few theoretical and experimental studies on the higher excited light vector mesons, so it is necessary to study their properties, which should be helpful in searching for them experimentally.

Recently, we have studied the mass spectra and strong decay properties of the excited ρ mesons $Y(2040)/\rho(2000)$, $\rho(1900)$, and $\rho(2150)$ with the modified Godfrey-Isgur (MGI) model and the $^3P_0$ model, where the Godfrey-Isgur model is modified by substituting the linear potential by the screened potential [17,18], and found that they can be assigned as $\rho(2^3D_1)$, $\rho(3^3S_1)$, and $\rho(4^3S_1)$, respectively [19]. We have also shown that the screening effects are crucial to promote theoretical descriptions of the of the spectra for the observed excited ρ mesons, as shown in Fig. 2 of Ref. [19]. We have predicted that the $Y(2040)$ mainly decays to $\pi\pi$ and $\pi\omega$, which is in good agreement with the measurements of the processes $p\bar{p} \to \pi\pi$ and $e^+e^- \to \omega\pi$ [5,20]. For $\rho(1900)$, the predicted main decay modes are $\pi\omega$ and $a_2(1320)\pi$, which is also consistent with the experimental measurements [3]. For $\rho(2150)$, its main decay modes are expected to be $\pi\pi$, $\pi\omega(1420)(\to 6\pi)$, and $\pi a_2(1320)(\to 6\pi)$, which is consistent with the experimental results [3]. Based on the successful descriptions of the excited mesons $Y(2040)/\rho(2000)$, $\rho(1900)$, and $\rho(2150)$, we would like to extend our study to the higher excited ρ mesons with masses above 2.4 GeV in this work.

Although the higher excited ρ mesons above 2.4 GeV have not been reported experimentally, there exist some hints of them in the experimental measurements. For instance, in 2002, Anisovich *et al.* analyzed experimental data of the process $p\bar{p} \to \omega\eta\pi^0$ measured by the Crystal Barrel collaboration, and showed that there exists a peak structure with $J^{PC} = 1^{--}$ around 2.4 GeV [21]. Later in 2006, the *BABAR* collaboration reported the $\omega\pi^+\pi^-\pi^0$ energy-dependent reaction cross section, as shown in Fig. 18 of Ref. [22], where one can easily find a peak around 2.6 GeV, which may be the higher excited ρ meson according to the G parity conservation.

In 2007, the *BABAR* collaboration presented the cross section of the process $e^+e^- \to K^+K^-\pi^+\pi^-\pi^0$, where there is a peak structure around 2.5 GeV [23]. The analysis of the *BABAR* measurements within the vector meson dominance model shows the existences of the $\rho(1900)$ and another resonance with mass of $M = 2550 \pm 13$ MeV and width of $\Gamma = 209 \pm 26$ MeV [24], where the latter one is expected to have the same quantum numbers as $\rho(1900)$. In addition, the cross sections of $e^+e^- \to \eta'\pi^+\pi^-$ and $e^+e^- \to f_1(1285)\pi^+\pi^-$ processes reported by *BABAR* indicate that

*lidm@zzu.edu.cn
†songqintao@zzu.edu.cn
‡wangen@zzu.edu.cn
§yanwc@zzu.edu.cn

there exist some structures around 2.5 GeV, although it is difficult to claim the existences of new resonances due to the insufficient data statistics [23].

In a word, there exist some hints of the higher excited ρ mesons according to the above experimental measurements, as pointed out in Ref. [25], and the existences of the higher excited ρ mesons above 2.4 GeV need to be confirmed by more precise experimental measurements in future. The theoretical predictions for their mass spectra and decay properties are crucial to search for them experimentally. Thus, we will study the mass spectra and decay properties of the higher excited ρ mesons above 2.4 GeV with the MGI model and the $^3P_0$ strong decay model, as used in our previous work [19].

The organization of this paper is as follows. First we introduce the MGI model and the $^3P_0$ model in Secs. II and III, respectively. Then we present the numerical results of the mass spectra and strong decays for the higher excited ρ mesons in Sec. IV. Finally a short summary is given in Sec. V.

II. RELATIVISTIC QUARK MODEL

The Godfrey-Isgur relativistic quark model (GI model) was proposed in 1985 by Godfrey and Isgur [26], and is widely used in describing the mass spectra of mesons [27–29], especially for the lower excited mesons. However, the masses of the higher excited mesons measured by experiments are much lower than the predictions of the GI model. Many studies show that the screening effects play an important role in studying the higher radial and orbital excited mesons [17,18], and we adopt the MGI model, which involves the screening effects, to calculate the mass spectra of the high excited ρ mesons. First we present a brief introduction of the GI model and the MGI model.

A. GI model

Within the GI model, the Hamiltonian of the meson's internal interaction can be written as [26]

$$\tilde{H} = \sqrt{m_1^2 + \mathbf{p}^2} + \sqrt{m_2^2 + \mathbf{p}^2} + \tilde{V}_{\text{eff}}(\mathbf{p}, \mathbf{r}), \tag{1}$$

where m_1 and m_2 denote the masses of quark and antiquark in the meson, respectively, $\mathbf{p} = \mathbf{p}_1 = -\mathbf{p}_2$ is the center-of-mass momentum, and $\mathbf{r}$ corresponds to the spatial coordinate. The $\tilde{V}_{\text{eff}}(\mathbf{p}, \mathbf{r})$ is the effective potential between quark and antiquark and can be expressed as follows in the nonrelativistic limit:

$$V_{\text{eff}}(r) = H^{\text{conf}} + H^{\text{hyp}} + H^{\text{so}}, \tag{2}$$

where H^{conf} is the spin-independent potential and includes the spin-independent linear confinement and Coulomb-type interaction:

$$\begin{aligned} H^{\text{conf}} &= \left[-\frac{3}{4}(c + br) + \frac{\alpha_s(r)}{r}\right]\boldsymbol{F}_1 \cdot \boldsymbol{F}_2, \\ &= S(r) + G(r), \end{aligned} \tag{3}$$

where $\langle \boldsymbol{F}_1 \cdot \boldsymbol{F}_2 \rangle = -4/3$ for a meson. $\alpha_s(Q^2)$ is the running coupling constant of QCD, which depends on the energy scale Q. $\alpha_s(Q^2)$ is divergent at low Q region. The authors of Ref. [26] assume that $\alpha_s(Q^2)$ saturates as $\alpha_s(Q^2 = 0) = \alpha_s^{\text{critital}}$, which is regarded as a parameter to be determined by fitting to experimental data. $\alpha_s(r)$ is obtained from $\alpha_s(Q^2)$ by using Fourier transform, where r is the relative distance between quark and antiquark. H^{hyp} denotes the color-hyperfine interaction,

$$\begin{aligned} H^{\text{hyp}} = -\frac{\alpha_s(r)}{m_1 m_2}\Bigg[\frac{1}{r^3}\left(\frac{3\boldsymbol{S}_1 \cdot \boldsymbol{r}\boldsymbol{S}_2 \cdot \boldsymbol{r}}{r^2} - \boldsymbol{S}_1 \cdot \boldsymbol{S}_2\right) \\ + \frac{8\pi}{3}\boldsymbol{S}_1 \cdot \boldsymbol{S}_2 \delta^3(\boldsymbol{r})\Bigg]\boldsymbol{F}_1 \cdot \boldsymbol{F}_2. \end{aligned} \tag{4}$$

H^{so} is the spin-orbit interaction that contains the color-magnetic term $H^{\text{so(cm)}}$ and the Thomas-precession term $H^{\text{so(tp)}}$,

$$H^{\text{so}} = H^{\text{so(cm)}} + H^{\text{so(tp)}}, \tag{5}$$

$$H^{\text{so(cm)}} = \frac{-\alpha_s(r)}{r^3}\left(\frac{1}{m_2} + \frac{1}{m_2}\right)\left(\frac{\boldsymbol{S}_1}{m_1} + \frac{\boldsymbol{S}_2}{m_2}\right) \cdot \boldsymbol{L}(\boldsymbol{F}_1 \cdot \boldsymbol{F}_2), \tag{6}$$

$$H^{\text{so(tp)}} = -\frac{1}{2r}\frac{\partial H^{\text{conf}}}{\partial r}\left(\frac{\boldsymbol{S}_1}{m_1^2} + \frac{\boldsymbol{S}_2}{m_2^2}\right) \cdot \boldsymbol{L}. \tag{7}$$

The spin-orbit interaction will give rise to the mixing between spin singlet ^1L_J and spin triplet ^3L_J if $m_1 \neq m_2$.

In GI model, the relativistic effects are introduced by two main ways. First, in the quark-antiquark scattering, the interactions should depend on both quark momentum $\vec{p}_1$ and antiquark momentum $\vec{p}_2$, or a linear combination of them as $\vec{p}_1 - \vec{p}_2$ and $\vec{p}_1 + \vec{p}_2$, so they must be nonlocal interaction potentials as pointed out in Ref. [26]. In order to take this effect into account, a smearing function $\rho_{12}(\mathbf{r} - \mathbf{r}')$ is used to transform the basic potentials $G(r)$ and $S(r)$ into the smeared ones $\tilde{G}(r)$ and $\tilde{S}(r)$, the specific form is

$$\tilde{f}(r) = \int d^3r' \rho_{12}(\mathbf{r} - \mathbf{r}') f(r'), \tag{8}$$

and the smearing function $\rho_{12}(\mathbf{r} - \mathbf{r}')$ is defined as

$$\rho_{12}(\mathbf{r} - \mathbf{r}') = \frac{\sigma_{12}^3}{\pi^{3/2}} e^{-\sigma_{12}^2(\mathbf{r}-\mathbf{r}')^2}, \tag{9}$$

$$\sigma_{12}^2=\sigma_0^2\left[\frac{1}{2}+\frac{1}{2}\left(\frac{4m_1m_2}{(m_1+m_2)^2}\right)^4\right]+s^2\left(\frac{2m_1m_2}{m_1+m_2}\right)^2. \quad (10)$$

For a heavy-heavy $Q\bar{Q}$ meson system, $\rho_{12}(\mathbf{r}-\mathbf{r}')$ will turn into delta function $\delta^3(\mathbf{r}-\mathbf{r}')$ as one increases the quark mass m_Q, in this case, one can obtain $\tilde{f}(r)=f(r)$, which indicates that the relativistic effects can be neglected for a heavy-heavy $Q\bar{Q}$ meson. However, the relativistic effects are important for heavy-light mesons and light mesons; therefore, it is necessary to consider relativistic effects in the study of excited ρ mesons.

Second, the momentum-dependent factors are introduced to modify the effective potentials, as shown in the following formula:

$$\tilde{G}(r)\to\left(1+\frac{p^2}{E_1E_2}\right)^{1/2}\tilde{G}(r)\left(1+\frac{p^2}{E_1E_2}\right)^{1/2}, \quad (11)$$

$$\frac{\tilde{V}_i(r)}{m_1m_2}\to\left(\frac{m_1m_2}{E_1E_2}\right)^{1/2+\epsilon_i}\frac{\tilde{V}_i(r)}{m_1m_2}\left(\frac{m_1m_2}{E_1E_2}\right)^{1/2+\epsilon_i}, \quad (12)$$

where $\tilde{G}(r)$ is the Coulomb-type potential, and $\tilde{V}_i(r)$ represents the contact, tensor, vector spin-orbit, and scalar spin-orbit terms as explained in Ref. [26]. In the nonrelativistic limit, those momentum-dependent factors will become unity.

With the help of the detailed expressions of Eq. (1), we could obtain the mass spectra and wave functions of mesons by solving the Schrödinger equation with the Gaussian expansion method, and the meson wave functions are used as inputs to investigate the subsequent strong decays for mesons.

B. MGI model involving the screening effects

In GI model, the linear potential br tends to infinity with the increasing of the distance between quark and antiquark, however for the large distance, the quark-antiquark pairs are generated in the vacuum, and the colors of quark and antiquark are screened in a meson, which implies that the simple linear potential br cannot accurately describe the interaction between quarks for higher excited mesons [17,18,30,31]. The study of the lattice QCD shows that the effective potential of mesons deviates from the traditional linear potential when the distance between quark and antiquark is greater than 1 fm [32]. Therefore, it is very important to introduce the screening effects when studying the masses of higher radial and orbital excited mesons.

The screening effects are introduced to the GI model by substituting linear potential br with the following form [17,18,30]:

$$V(r)=br\to V^{\rm scr}(r)=\frac{b(1-e^{-\mu r})}{\mu}, \quad (13)$$

TABLE I. Parameter values in the MGI model [27].

Parameter	Value	Parameter	Value
m_u (GeV)	0.163	s	1.497
m_d (GeV)	0.163	μ (GeV)	0.0635
m_s (GeV)	0.387	$\epsilon_{\rm c}$	−0.138
b (GeV^2)	0.221	$\epsilon_{\rm sov}$	0.157
c (GeV)	−0.240	$\epsilon_{\rm sos}$	0.9726
σ_0 (GeV)	1.799	$\epsilon_{\rm t}$	0.893

when r is small enough, we can have $V^{\rm scr}(r)=V(r)$; therefore, this replacement will not affect the lower-lying meson states. The parameter μ is related to the strength of the screening effects and can be determined by fitting to the experimental data.

Furthermore, the smeared potential of Eq. (8) can be rewritten as [30,33]

$$\begin{aligned}\tilde{V}^{\rm scr}(r)=\frac{b}{\mu r}\Bigg[&e^{\frac{\mu^2}{4\sigma^2}+\mu r}\left(\frac{1}{\sqrt{\pi}}\int_0^{\frac{\mu+2r\sigma^2}{2\sigma}}e^{-x^2}dx-\frac{1}{2}\right)\\&\times\frac{\mu+2r\sigma^2}{2\sigma^2}+r-e^{\frac{\mu^2}{4\sigma^2}-\mu r}\frac{\mu-2r\sigma^2}{2\sigma^2}\\&\times\left(\frac{1}{\sqrt{\pi}}\int_0^{\frac{\mu-2r\sigma^2}{2\sigma}}e^{-x^2}dx-\frac{1}{2}\right)\Bigg],\end{aligned} \quad (14)$$

where $\sigma=\sigma_{12}$ is defined in Eq. (10).

The MGI model is widely used in the studies of mass spectrum of heavy-heavy mesons, heavy-light mesons, and light mesons [12,19,27,30,33–39]. The parameters of the MGI model are taken from Ref. [27], as tabulated in Table I. The values of other parameters can be found in Ref. [26].

III. $^3P_0$ STRONG DECAY MODEL

In addition to the mass spectrum, the strong decay properties are crucial for experiments to search for the higher excited ρ mesons. Here, we give a brief introduction of the $^3P_0$ model, which is widely used in studying two-body Okubo-Zweig-Iizuka (OZI)-allowed strong decays of mesons [8,36,40–42].

The $^3P_0$ model was originally proposed by Micu [43] in 1968, and later it was further developed by Le Yaouanc *et al.* [44,45]. The $^3P_0$ model has been considered as an effective tool to study two-body OZI-allowed strong decays of hadrons. For the process $A\to B+C$, the main idea of the $^3P_0$ model is that a flavor-singlet and color-singlet quark-antiquark pair with $J^{PC}=0^{++}$ is created from the vacuum firstly, then, the created antiquark (quark) combines with the quark (antiquark) in meson A to form meson $B(C)$ as shown in Figs. 1(a) and 1(b).

The transition operator T of the decay $A\to B+C$ in the $^3P_0$ model is given by [46]

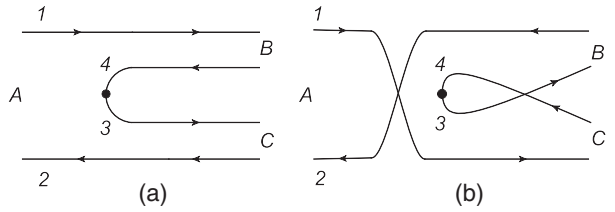

FIG. 1. Two possible diagrams contributing to the process $A \to B + C$ in the $^3P_0$ model. (a) The created antiquark (quark) combines with the quark (antiquark) of meson A to form meson $B(C)$, (b) the created antiquark (quark) combines with the quark (antiquark) of meson A to form meson $C(B)$.

$$T = -3\gamma\sum_m \langle 1m1-m|00\rangle \int d^3\boldsymbol{p}_3 d^3\boldsymbol{p}_4 \delta^3(\boldsymbol{p}_3+\boldsymbol{p}_4) \times \mathcal{Y}_1^m\left(\frac{\boldsymbol{p}_3-\boldsymbol{p}_4}{2}\right)\chi^{34}_{1,-m}\phi_0^{34}\omega_0^{34}b_3^\dagger(\boldsymbol{p}_3)d_4^\dagger(\boldsymbol{p}_4), \quad (15)$$

where $\boldsymbol{p}_3(\boldsymbol{p}_4)$ is the momentum of the created quark (antiquark). The dimensionless parameter γ stands for the strength of the quark-antiquark $q_3\bar{q}_4$ pair created from the vacuum, and is usually determined by fitting to the experimental data. $\chi^{34}_{1,-m}$, ϕ_0^{34}, and ω_0^{34} are spin, flavor, and color wave functions of the created quark-antiquark pair, respectively.

With the transition operator T, the helicity amplitude $\mathcal{M}^{M_{J_A}M_{J_B}M_{J_C}}(\boldsymbol{P})$ can be written as

$$\langle BC|T|A\rangle = \delta^3(\boldsymbol{P}_A-\boldsymbol{P}_B-\boldsymbol{P}_C)\mathcal{M}^{M_{J_A}M_{J_B}M_{J_C}}(\boldsymbol{P}), \quad (16)$$

where $|A\rangle$, $|B\rangle$, and $|C\rangle$ denote the mock meson states defined in Ref. [47], and $\boldsymbol{P}$ is the momentum of meson B in the center of mass frame. Then the helicity amplitude is obtained as

$$\mathcal{M}^{M_{J_A}M_{J_B}M_{J_C}}(\boldsymbol{P}) = \gamma\sqrt{8E_AE_BE_C}\sum_{\substack{M_{L_A},M_{S_A},\\ M_{L_B},M_{S_B},\\ M_{L_C},M_{S_C},m}} \langle L_AM_{L_A}S_AM_{S_A}|J_AM_{J_A}\rangle\langle L_BM_{L_B}S_BM_{S_B}|J_BM_{J_B}\rangle\langle L_CM_{L_C}S_CM_{S_C}|J_CM_{J_C}\rangle \times \langle 1m1-m|00\rangle\langle\chi^{14}_{S_BM_{S_B}}\chi^{32}_{S_CM_{S_C}}|\chi^{12}_{S_AM_{S_A}}\chi^{34}_{1-m}\rangle[f_1I(\boldsymbol{P},m_1,m_2,m_3)+(-1)^{1+S_A+S_B+S_C}f_2I(-\boldsymbol{P},m_2,m_1,m_3)], \quad (17)$$

where $f_1 = \langle\phi_B^{14}\phi_C^{32}|\phi_A^{12}\phi_0^{34}\rangle$ and $f_2 = \langle\phi_B^{32}\phi_C^{14}|\phi_A^{12}\phi_0^{34}\rangle$ correspond to the flavor superposition of the two combinations depicted in Figs. 1(a) and 1(b), respectively. The momentum space integral $I(\boldsymbol{P},m_1,m_2,m_3)$ is given by

$$I(\boldsymbol{P},m_1,m_2,m_3) = \int d^3\boldsymbol{p}\psi^*_{n_BL_BM_{L_B}}\left(\frac{m_3}{m_1+m_3}\boldsymbol{P_B}+\boldsymbol{p}\right)\psi^*_{n_CL_CM_{L_C}}\left(\frac{m_3}{m_2+m_3}\boldsymbol{P_B}+\boldsymbol{p}\right)\psi_{n_AL_AM_{L_A}}(\boldsymbol{P_B}+\boldsymbol{p})\mathcal{Y}_1^m(\boldsymbol{p}). \quad (18)$$

Furthermore, the partial wave amplitude $\mathcal{M}^{LS}(\boldsymbol{P})$ for the decay $A \to B + C$ can be expressed as [48]

$$\mathcal{M}^{LS}(\boldsymbol{P}) = \sum_{\substack{M_{J_B},M_{J_C},\\ M_S,M_L}} \langle LM_LSM_S|J_AM_{J_A}\rangle\langle J_BM_{J_B}J_CM_{J_C}|SM_S\rangle \int d\Omega Y^*_{LM_L}\mathcal{M}^{M_{J_A}M_{J_B}M_{J_C}}(\boldsymbol{P}). \quad (19)$$

Finally, within the relativistic phase space, the total width $\Gamma(A \to B + C)$ can be expressed in terms of the partial wave amplitude squared [46]

$$\Gamma(A \to B + C) = \frac{\pi|\boldsymbol{P}|}{4M_A^2}\sum_{LS}|\mathcal{M}^{LS}(\boldsymbol{P})|^2, \quad (20)$$

where $|\boldsymbol{P}| = \frac{\sqrt{[M_A^2-(M_B+M_C)^2][M_A^2-(M_B-M_C)^2]}}{2M_A}$, M_A, M_B, and M_C are the masses of the mesons A, B, and C, respectively.

IV. NUMERICAL RESULTS

A. Mass spectrum analysis

First, we have calculated the masses of the higher excited ρ mesons within the MGI and GI models, which are shown in Table II. There are six higher excited ρ mesons in the region of 2.4–3.0 GeV, which are $\rho(5^3S_1)$, $\rho(6^3S_1)$, $\rho(7^3S_1)$, $\rho(4^3D_1)$, $\rho(5^3D_1)$, and $\rho(6^3D_1)$. The deviations

TABLE II. Masses of the higher excited ρ mesons predicted by the GI and MGI models.

State	MGI (MeV)	GI (MeV)
$\rho(5^3S_1)$	2542	2817
$\rho(6^3S_1)$	2774	3160
$\rho(7^3S_1)$	2967	3470
$\rho(4^3D_1)$	2624	2915
$\rho(5^3D_1)$	2840	3239
$\rho(6^3D_1)$	3020	3554

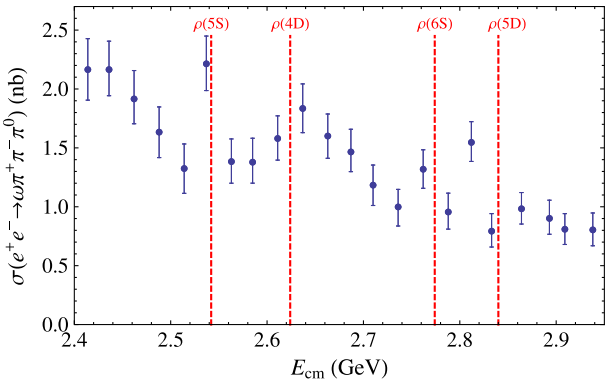

FIG. 2. Comparison of the masses of the higher excited ρ mesons predicted by MGI model with the shape of the cross section of the process $e^+e^- \to \omega\pi^+\pi^-\pi^0$ reported by *BABAR*. The red dotted lines are masses predicted with MGI model, and the blue data points are the *BABAR* experimental data.

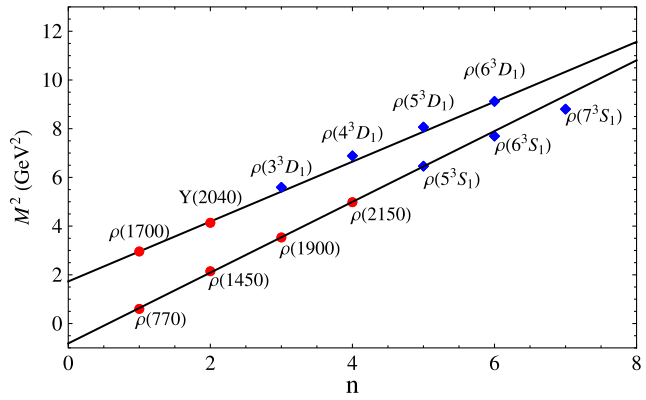

FIG. 3. The Regge trajectories for the $\rho(n^3S_1)$ and $\rho(n^3D_1)$ masses, where the parameters $M_0^2 = 0.64$ GeV^2 and $\mu^2 = 1.45$ GeV^2 for $\rho(n^3S_1)$, and $M_0^2 = 2.96$ GeV^2 and $\mu^2 = 1.23$ GeV^2 for $\rho(n^3D_1)$.

between the predictions of MGI and GI models are about 300–500 MeV, which implies that the screening potential plays an important role in studying the masses of the higher excited ρ mesons. It should be pointed out that the MGI model has also been adopted to study the spectra of the ϕ mesons [11], the B mesons [31], charmonia [36], charmed mesons [33], and charmed-strange mesons [30], and give a better descriptions for the spectra, which makes our predictions for the high excited ρ mesons more reliable.

The recent analyses of the *BABAR* measurements about the process $e^+e^- \to K^+K^-\pi^+\pi^-\pi^0$ indicate the existence of one resonance with mass $M = (2550 \pm 13)$ MeV [24], which is in good agreement with our predicted mass of $\rho(5^3S_1)$. In addition, the cross section of the process $e^+e^- \to \omega\pi^+\pi^-\pi^0$ measured by *BABAR* indicates that there are hints of the higher excited ρ mesons. From Fig. 2, one can find one datum point around 2.54 GeV, very close to our predicted mass 2542 MeV of $\rho(5^3S_1)$, and an enhancement structure around 2.64 GeV, which could be related to the state $\rho(4^3D_1)$ with a mass of 2624 MeV. Another datum point appears around 2.76 GeV, close to the predicted mass of $\rho(6^3S_1)$. Although some hints of the higher excited ρ mesons exist, one cannot claim those resonances due to the poor quality of the present data, and the more accurate measurements in future are crucial to confirm the existence of these resonances.

In addition, the light mesons with different radial excitation could be well fit to the following quasilinear (n, M^2) Regge trajectories [49],

$$M_n^2 = M_0^2 + (n-1)\mu^2, \tag{21}$$

where M_n stands for the mass of the meson with radial quantum number n, and M_0^2 and μ^2 are the parameters of the trajectories. With the assignments of $\rho(770)$ as $\rho(1^3S_1)$, $\rho(1450)$ as $\rho(2^3S_1)$, $\rho(1900)$ as $\rho(3^3S_1)$, $\rho(1700)$ as $\rho(1^1D_1)$, and $Y(2040)$ as $\rho(2^3D_1)$, respectively, we obtain the parameters $M_0^2 = 0.64$ GeV^2 and $\mu^2 = 1.45$ GeV^2 for S-wave ρ mesons, and $M_0^2 = 2.96$ GeV^2 and $\mu^2 = 1.23$ GeV^2 for D-wave ρ mesons. We plot the Regge trajectories in Fig. 3, and tabulate masses in Table III. The two trajectories of S wave and D wave are not quite parallel because their slops are different. It should be stressed that the trajectories slopes for S wave and D wave could be different, for instance, in Ref. [11] the slope is $\mu^2 = 1.5$ GeV^2 for S-wave ω/ρ meson family, and $\mu^2 = 1.05$ GeV^2 for D-wave ω/ρ meson family. It should be pointed out that the mass predictions of Regge trajectories are in good agreement with the measured masses of ρ mesons and the MGI predictions.

B. Decay behavior analysis

In this work, we employ the $^3P_0$ model with the realistic meson wave functions obtained from the MGI model to evaluate the decay widths of $\rho(5^3S_1)$, $\rho(4^3D_1)$, $\rho(6^3S_1)$,

TABLE III. Comparison of the measured masses of ρ mesons to the predictions of the Regge trajectories and the MGI model.

$n^{2S+1}L_J$	State	RPP (MeV) [3]	MGI (MeV)	Regge (MeV)
$\rho(1^3S_1)$	$\rho(770)$	775.26 ± 0.23	774	798
$\rho(2^3S_1)$	$\rho(1450)$	1465 ± 25	1424	1445
$\rho(3^3S_1)$	$\rho(1900)$	1880 ± 30	1906	1882
$\rho(4^3S_1)$	$\rho(2150)$	$2232 \pm 8 \pm 9$	2259	2235
$\rho(5^3S_1)$			2542	2539
$\rho(6^3S_1)$			2774	2810
$\rho(7^3S_1)$			2967	3058
$\rho(1^3D_1)$	$\rho(1700)$	1720 ± 20	1646	1720
$\rho(2^3D_1)$	$Y(2040)$	$2034 \pm 13 \pm 9$	2048	2046
$\rho(3^3D_1)$			2365	2327
$\rho(4^3D_1)$			2624	2578
$\rho(5^3D_1)$			2840	2806
$\rho(6^3D_1)$			3020	3017

TABLE IV. The decay widths of $\rho(5^3S_1)$ (in MeV), the initial state mass is set to be 2542 MeV and the masses of the final states are taken from RPP [3]. (Note: the widths presented in this table and the following tables are straightly calculated, and the numbers with the level of 0.01 MeV do not correspond to precision).

Channel	Mode	$\rho(5^3S_1)$	Mode	$\rho(5^3S_1)$
$1^-\to 0^-0^-$	$\pi\pi$	2.52	KK	<0.01
	$\pi\pi(1300)$	12.71	$KK(1460)$	0.01
	$\pi\pi(1800)$	9.28		
$1^-\to 0^-1^-$	$\pi\omega$	0.81	$KK^*(1680)$	0.01
	$\rho\eta$	0.03	$\rho(1700)\eta$	0.09
	$\omega(1420)\pi$	11.07	$\rho\eta(1475)$	0.17
	$\omega(1650)\pi$	0.11	$\omega\pi(1300)$	1.02
	KK^*	0.02	$\rho\eta(1295)$	0.67
	$KK^*(1410)$	<0.01	$\rho(1450)\eta$	0.65
	$\rho\eta'$	0.14		
$1^-\to 1^-1^-$	$\rho\rho$	5.64	K^*K^*	0.15
	$\rho\rho(1450)$	12.93	$K^*K^*(1410)$	0.49
$1^-\to 0^-1^+$	$a_1(1260)\pi$	3.26	$b_1(1235)\eta'$	0.17
	$h_1(1170)\pi$	4.22	$\pi a_1(1640)$	9.81
	$KK_1(1400)$	0.10	$b_1(1235)\eta$	0.49
	$KK_1(1270)$	0.10		
$1^-\to 0^-2^+$	$a_2(1320)\pi$	4.83	$a_2(1700)\pi$	27.80
	$KK_2^*(1430)$	0.01		
$1^-\to 0^-2^-$	$\pi\pi_2(1670)$	3.65	$\pi\eta_2(1645)$	1.94
	$KK_2(1770)$	0.02	$KK_2(1820)$	0.03
$1^-\to 0^-3^-$	$\pi\omega_3(1670)$	2.46	$\eta\rho_3(1690)$	0.02
	$KK_3(1780)$	<0.01		
$1^-\to 1^-1^+$	$b_1(1235)\rho$	3.38	$K_1(1400)K^*$	0.02
	$a_1(1260)\omega$	3.14	$K_1(1270)K^*$	0.09
	$\rho f_1(1285)$	3.00	$\rho f_1(1420)$	0.16
	$\rho h_1(1170)$	2.50		
$1^-\to 2^+1^-$	$\rho f_2(1270)$	3.93	$K^*K_2^*(1430)$	0.03
	$\omega a_2(1320)$	5.10		
$1^-\to 0^-4^+$	$a_4(1970)\pi$	0.91		
$1^-\to 1^-0^+$	$a_0(1450)\omega$	0.52		
Total width		143.01		

TABLE V. The decay widths of $\rho(4^3D_1)$ (in MeV), the initial state mass is set to be 2624 MeV and the masses of all the final states are taken from PRR [3].

Channel	Mode	$\rho(4^3D_1)$	Mode	$\rho(4^3D_1)$
$1^-\to 0^-0^-$	$\pi\pi$	5.55	KK	<0.01
	$\pi\pi(1300)$	11.16	$KK(1460)$	<0.01
	$\pi\pi(1800)$	7.07		
$1^-\to 0^-1^-$	$\pi\omega$	0.48	$KK^*(1680)$	0.01
	$\rho\eta$	0.07	$\rho(1700)\eta$	0.07
	$\omega(1420)\pi$	2.23	$\rho\eta(1475)$	<0.01
	$\omega(1650)\pi$	0.23	$\omega\pi(1300)$	0.61
	KK^*	0.01	$\rho\eta(1295)$	0.36
	$KK^*(1410)$	<0.01	$\rho(1450)\eta$	0.37
	$\rho\eta'$	0.14		
$1^-\to 1^-1^-$	$\rho\rho$	4.81	K^*K^*	0.02
	$\rho\rho(1450)$	14.42	$K^*K^*(1410)$	0.06
$1^-\to 0^-1^+$	$a_1(1260)\pi$	4.00	$b_1(1235)\eta'$	0.10
	$h_1(1170)\pi$	6.90	$\pi a_1(1640)$	10.54
	$KK_1(1400)$	0.04	$b_1(1235)\eta$	0.82
	$KK_1(1270)$	0.05		
$1^-\to 0^-2^+$	$a_2(1320)\pi$	0.96	$a_2(1700)\pi$	7.09
	$KK_2^*(1430)$	<0.01		
$1^-\to 0^-2^-$	$\pi\pi_2(1670)$	6.02	$\pi\eta_2(1645)$	4.48
	$KK_2(1770)$	0.05	$KK_2(1820)$	0.01
$1^-\to 0^-3^-$	$\pi\omega_3(1670)$	1.35	$\eta\rho_3(1690)$	0.10
	$KK_3(1780)$	<0.01		
$1^-\to 1^-1^+$	$b_1(1235)\rho$	1.15	$K_1(1400)K^*$	0.04
	$a_1(1260)\omega$	0.39	$K_1(1270)K^*$	0.08
	$\rho f_1(1285)$	0.52	$\rho f_1(1420)$	0.14
	$\rho h_1(1170)$	1.14		
$1^-\to 2^+1^-$	$\rho f_2(1270)$	5.71	$K^*K_2^*(1430)$	0.01
	$\omega a_2(1320)$	3.58		
$1^-\to 0^-4^+$	$a_4(1970)\pi$	0.40		
$1^-\to 1^-0^+$	$a_0(1450)\omega$	0.60		
Total width		105.82		

$\rho(5^3D_1)$, $\rho(7^3S_1)$, and $\rho(6^3D_1)$. The value of parameter γ is taken from our previous work [19], where it was obtained by fitting to the decay widths of the light mesons with same quantum numbers as ρ mesons. $\gamma = 6.57 \pm 0.25$ is used for the $u\bar{u}/d\bar{d}$ pair creation, and the γ value of $s\bar{s}$ pair creation is suppressed by an additional factor m_u/m_s. The predicted masses by the MGI model are used for the unobserved excited ρ mesons in the calculations of the strong decay widths, and the masses of the other mesons are taken from "Review of Particle Physics" (RPP) [3]. Due to the broken of the SU(3) flavor symmetry, $K_1(1^1P_1)$ and $K_1(1^3P_1)$ do not possess definite C parity. These two state can in principle mix to give the physical $K_1(1270)$ and $K_1(1400)$,

$$K_1(1270) = \sin\theta_{K_1} K_1(1^3P_1) + \cos\theta_{K_1} K_1(1^1P_1),$$
$$K_1(1400) = \cos\theta_{K_1} K_1(1^3P_1) - \sin\theta_{K_1} K_1(1^1P_1), \quad (22)$$

with the mixing angle $\theta_{K_1} = 34°$ [50].

The partial widths and total width of $\rho(5^3S_1)$ are listed in Table IV.[1] The total decay width of $\rho(5^3S_1)$ is expected to be $\Gamma = 143$ MeV, which is close to the lower limit of the width $\Gamma = (209 \pm 26)$ MeV obtained in Ref. [24]. The main decay modes of $\rho(5^3S_1)$ are $\pi\pi(1300)(\to 4\pi)$, $\pi\pi(1800)(\to 4\pi)$, $\pi\omega(1420)(\to 4\pi, 6\pi)$, $\rho\rho(1450)(\to 4\pi, 6\pi)$, $\pi a_1(1640)(\to 4\pi)$, and $\pi a_2(1700)(\to \eta\pi\pi, \pi K\bar{K})$, thus one can search for the $\rho(5^3S_1)$ in the channels of $4\pi, 6\pi, \eta\pi\pi$, and $\pi K\bar{K}$.

The partial widths and total width of $\rho(4^3D_1)$ are listed in Table V. The total decay width of $\rho(4^3D_1)$ is expected to be $\Gamma = 105.82$ MeV, consistent with the broad structure around 2.64 GeV in Fig. 2. The predicted main decay modes are $\pi\pi(1300)(\to 4\pi)$, $\pi\pi(1800)(\to 4\pi)$, $\rho\rho(1450)(\to 4\pi)$, $\pi h_1(1170)(\to 4\pi)$, $\pi a_1(1640)(\to 4\pi)$,

[1]It should be stressed that the widths presented in Tables IV–IX are straightly calculated, and the uncertainties of our results will be discussed in the end of this section.

TABLE VI. The decay widths of $\rho(6^3S_1)$ (in MeV), the initial state mass is set to be 2774 MeV and the masses of all the final states are taken from RPP [3].

Channel	Mode	$\rho(6^3S_1)$	Mode	$\rho(6^3S_1)$
$1^-\to 0^-0^-$	$\pi\pi$	0.51	KK	<0.01
	$\pi\pi(1300)$	4.83	$KK(1460)$	<0.01
	$\pi\pi(1800)$	5.36		
$1^-\to 0^-1^-$	$\pi\omega$	<0.01	$KK^*(1680)$	<0.01
	$\rho\eta$	0.02	$\rho(1700)\eta$	0.04
	$\omega(1420)\pi$	3.29	$\rho\eta(1475)$	0.12
	$\omega(1650)\pi$	0.03	$\omega\pi(1300)$	0.21
	KK^*	<0.01	$\rho\eta(1295)$	0.14
	$KK^*(1410)$	0.01	$\rho(1450)\eta$	0.10
	$\rho\eta'$	0.08		
$1^-\to 1^-1^-$	$\rho\rho$	3.67	K^*K^*	<0.01
	$\rho\rho(1450)$	7.26	$K^*K^*(1410)$	0.10
$1^-\to 0^-1^+$	$a_1(1260)\pi$	0.59	$b_1(1235)\eta'$	0.09
	$h_1(1170)\pi$	0.79	$\pi a_1(1640)$	5.44
	$KK_1(1400)$	0.02	$b_1(1235)\eta$	0.08
	$KK_1(1270)$	0.02		
$1^-\to 0^-2^+$	$a_2(1320)\pi$	0.36	$a_2(1700)\pi$	13.82
	$KK_2^*(1430)$	<0.01		
$1^-\to 0^-2^-$	$\pi\pi_2(1670)$	0.95	$\pi\eta_2(1645)$	0.59
	$KK_2(1770)$	<0.01	$KK_2(1820)$	<0.01
$1^-\to 0^-3^-$	$\pi\omega_3(1670)$	0.63	$\eta\rho_3(1690)$	<0.01
	$KK_3(1780)$	<0.01		
$1^-\to 1^-1^+$	$b_1(1235)\rho$	2.57	$K_1(1400)K^*$	<0.01
	$a_1(1260)\omega$	1.78	$K_1(1270)K^*$	0.01
	$\rho f_1(1285)$	1.68	$\rho f_1(1420)$	0.10
	$\rho h_1(1170)$	1.94		
$1^-\to 2^+1^-$	$\rho f_2(1270)$	4.12	$K^*K_2^*(1430)$	<0.01
	$\omega a_2(1320)$	4.36		
$1^-\to 0^-4^+$	$a_4(1970)\pi$	1.31		
$1^-\to 1^-0^+$	$a_0(1450)\omega$	0.36		
Total width		67.46		

TABLE VII. The decay widths of $\rho(5^3D_1)$ (in MeV), the initial state mass is set to be 2840 MeV and the masses of the final states are taken from RPP [3].

Channel	Mode	$\rho(5^3D_1)$	Mode	$\rho(5^3D_1)$
$1^-\to 0^-0^-$	$\pi\pi$	3.46	KK	<0.01
	$\pi\pi(1300)$	10.25	$KK(1460)$	<0.01
	$\pi\pi(1800)$	7.90		
$1^-\to 0^-1^-$	$\pi\omega$	0.04	$KK^*(1680)$	0.10
	$\rho\eta$	<0.01	$\rho(1700)\eta$	0.07
	$\omega(1420)\pi$	1.19	$\rho\eta(1475)$	0.01
	$\omega(1650)\pi$	0.20	$\omega\pi(1300)$	0.17
	KK^*	<0.01	$\rho\eta(1295)$	0.11
	$KK^*(1410)$	0.02	$\rho(1450)\eta$	0.10
	$\rho\eta'$	0.04		
$1^-\to 1^-1^-$	$\rho\rho$	0.58	K^*K^*	<0.01
	$\rho\rho(1450)$	5.44	$K^*K^*(1410)$	0.04
$1^-\to 0^-1^+$	$a_1(1260)\pi$	1.34	$b_1(1235)\eta'$	0.07
	$h_1(1170)\pi$	2.64	$\pi a_1(1640)$	7.35
	$KK_1(1400)$	0.02	$b_1(1235)\eta$	0.16
	$KK_1(1270)$	0.02		
$1^-\to 0^-2^+$	$a_2(1320)\pi$	0.84	$a_2(1700)\pi$	5.81
	$KK_2^*(1430)$	<0.01		
$1^-\to 0^-2^-$	$\pi\pi_2(1670)$	1.58	$\pi\eta_2(1645)$	1.68
	$KK_2(1770)$	0.01	$KK_2(1820)$	<0.01
$1^-\to 0^-3^-$	$\pi\omega_3(1670)$	0.62	$\eta\rho_3(1690)$	0.03
	$KK_3(1780)$	<0.01		
$1^-\to 1^-1^+$	$b_1(1235)\rho$	1.22	$K_1(1400)K^*$	0.01
	$a_1(1260)\omega$	0.69	$K_1(1270)K^*$	0.03
	$\rho f_1(1285)$	0.91	$\rho f_1(1420)$	0.12
	$\rho h_1(1170)$	0.93		
$1^-\to 2^+1^-$	$\rho f_2(1270)$	1.41	$K^*K_2^*(1430)$	<0.01
	$\omega a_2(1320)$	0.84		
$1^-\to 0^-4^+$	$a_4(1970)\pi$	0.52		
$1^-\to 1^-0^+$	$a_0(1450)\omega$	0.46		
Total width		59.00		

and $\pi\pi_1(1670)(\to 4\pi)$, thus one can search for $\rho(4^3D_1)$ in the 4π channel.

The partial widths and total width of $\rho(6^3S_1)$ are listed in Table VI. The total decay width of $\rho(6^3S_1)$ is expected to be $\Gamma = 67.46$ MeV, and the main decay modes are predicted to be $\pi\pi(1300)(\to 4\pi), \pi\pi(1800)(\to 4\pi), \rho\rho(1450)(\to 4\pi, 6\pi)$, $\pi a_2(1700)(\to \eta\pi\pi, \pi K\bar{K})$, $\rho f_2(1270)(\to 4\pi)$, and $\omega a_2(1320)$. Considering the width of the intermediate state $a_2(1320)$ is 107 ± 5 MeV, the $\rho(6^3S_1)$ state is expected to be observed in the $\omega a_2(1320)$ channel.

The partial widths and total width of $\rho(5^3D_1)$ are listed in Table VII. The total decay width of $\rho(5^3D_1)$ is expected to be $\Gamma = 59.00$ MeV, and the predicted main decay modes are $\pi\pi(1300)(\to 4\pi)$, $\pi\pi(1800)(\to 4\pi)$, $\rho\rho(1450)(\to 4\pi)$, and $\pi a_1(1640)(\to 4\pi)$. Thus $\rho(5^3D_1)$ is expected to be observed in the 4π channel.

The partial widths and total width of $\rho(7^3S_1)$ are listed in Table VIII. The total decay width of $\rho(7^3S_1)$ is expected to be $\Gamma = 61.37$ MeV, and the predicted main decay modes are $\pi\pi(1300)(\to 4\pi)$, $\pi\pi(1800)(\to 4\pi)$, $\rho\rho(\to 4\pi)$, $\rho\rho(1450)(\to 4\pi, 6\pi)$, $\pi a_2(1700)(\to 4\pi)$, $\pi a_1(1640)(\to 4\pi)$, and $\omega a_2(1320)$. Thus one can search for the $\rho(7^3S_1)$ state in the $\omega a_2(1320)$ and 4π channels.

The partial widths and total width of $\rho(6^3D_1)$ are listed in Table IX. The total decay width of $\rho(6^3D_1)$ is expected to be $\Gamma = 23.88$ MeV, and the predicted main decay modes are $\pi\pi(1300)(\to 4\pi)$, $\pi\pi(1800)(\to 4\pi)$, $\pi a_1(1640)(\to 4\pi)$, and $\pi a_2(1700)(\to 4\pi)$. The state $\rho(6^3D_1)$ is expected to be observed in the 4π channel.

Finally, we give some discussions about the uncertainties of the calculated widths. Indeed, the uncertainties mainly come from the fitted parameter γ. The $\gamma = 6.57 \pm 0.24$ is obtained by fitting to the widths of $\rho(1700)$, $K^*(1680)$, $\omega(1650)$, $\rho(1450)$, $K^*(1410)$, $\phi(1680)$, and $\omega(1420)$ [19], which will give the uncertainties for the decay widths,

$$\frac{\Delta\Gamma}{\Gamma} \sim \frac{\delta(\gamma^2)}{\gamma^2} = \frac{2\gamma\delta(\gamma)}{\gamma^2} = 7.3\%. \tag{23}$$

TABLE VIII. The decay widths of $\rho(7^3S_1)$ (in MeV), the initial state mass is set to be 2967 MeV and the masses of the final states are taken from RPP [3].

Channel	Mode	$\rho(7^3S_1)$	Mode	$\rho(7^3S_1)$
$1^- \to 0^-0^-$	$\pi\pi$	<0.01	KK	<0.01
	$\pi\pi(1300)$	4.24	$KK(1460)$	0.01
	$\pi\pi(1800)$	5.77		
$1^- \to 0^-1^-$	$\pi\omega$	0.16	$KK^*(1680)$	<0.01
	$\rho\eta$	0.16	$\rho(1700)\eta$	0.09
	$\omega(1420)\pi$	1.14	$\rho\eta(1475)$	0.12
	$\omega(1650)\pi$	0.16	$\omega\pi(1300)$	<0.01
	KK^*	<0.01	$\rho\eta(1295)$	<0.01
	$KK^*(1410)$	<0.01	$\rho(1450)\eta$	<0.01
	$\rho\eta'$	0.11		
$1^- \to 1^-1^-$	$\rho\rho$	6.86	K^*K^*	0.04
	$\rho\rho(1450)$	9.09	$K^*K^*(1410)$	<0.01
$1^- \to 0^-1^+$	$a_1(1260)\pi$	1.21	$b_1(1235)\eta'$	0.08
	$h_1(1170)\pi$	0.42	$\pi a_1(1640)$	4.28
	$KK_1(1400)$	0.01	$b_1(1235)\eta$	0.15
	$KK_1(1270)$	0.01		
$1^- \to 0^-2^+$	$a_2(1320)\pi$	<0.01	$a_2(1700)\pi$	6.86
	$KK_2^*(1430)$	0.02		
$1^- \to 0^-2^-$	$\pi\pi_2(1670)$	0.70	$\pi\eta_2(1645)$	0.55
	$KK_2(1770)$	0.01	$KK_2(1820)$	
$1^- \to 0^-3^-$	$\pi\omega_3(1670)$	0.04	$\eta\rho_3(1690)$	0.05
	$KK_3(1780)$	<0.01		
$1^- \to 1^-1^+$	$b_1(1235)\rho$	3.09	$K_1(1400)K^*$	<0.01
	$a_1(1260)\omega$	1.92	$K_1(1270)K^*$	<0.01
	$\rho f_1(1285)$	1.57	$\rho f_1(1420)$	0.06
	$\rho h_1(1170)$	3.21		
$1^- \to 2^+1^-$	$\rho f_2(1270)$	4.21	$K^*K_2^*(1430)$	0.02
	$\omega a_2(1320)$	3.72		
$1^- \to 0^-4^+$	$a_4(1970)\pi$	0.53		
$1^- \to 1^-0^+$	$a_0(1450)\omega$	0.24		
Total width		61.37		

TABLE IX. The decay widths of $\rho(6^3D_1)$ (in MeV): the initial state mass is set to be 3020 MeV and the masses of the final states are taken from RPP [3].

Channel	Mode	$\rho(6^3D_1)$	Mode	$\rho(6^3D_1)$
$1^- \to 0^-0^-$	$\pi\pi$	0.84	KK	<0.01
	$\pi\pi(1300)$	4.29	$KK(1460)$	<0.01
	$\pi\pi(1800)$	5.22		
$1^- \to 0^-1^-$	$\pi\omega$	<0.01	$KK^*(1680)$	<0.01
	$\rho\eta$	0.02	$\rho(1700)\eta$	0.03
	$\omega(1420)\pi$	0.40	$\rho\eta(1475)$	0.03
	$\omega(1650)\pi$	0.06	$\omega\pi(1300)$	0.02
	KK^*	<0.01	$\rho\eta(1295)$	0.01
	$KK^*(1410)$	0.01	$\rho(1450)\eta$	<0.01
	$\rho\eta'$	0.03		
$1^- \to 1^-1^-$	$\rho\rho$	0.37	K^*K^*	<0.01
	$\rho\rho(1450)$	0.47	$K^*K^*(1410)$	0.03
$1^- \to 1^-1^+$	$a_1(1260)\pi$	0.16	$b_1(1235)\eta'$	0.05
	$h_1(1170)\pi$	0.40	$\pi a_1(1640)$	2.90
	$KK_1(1400)$	<0.01	$b_1(1235)\eta$	<0.01
	$KK_1(1270)$	<0.01		
$1^- \to 0^-2^+$	$a_2(1320)\pi$	0.05	$a_2(1700)\pi$	2.93
	$KK_2^*(1430)$	<0.01		
$1^- \to 0^-2^-$	$\pi\pi_2(1670)$	0.14	$\pi\eta_2(1645)$	0.16
	$KK_2(1770)$	<0.01	$KK_2(1820)$	<0.01
$1^- \to 0^-3^-$	$\pi\omega_3(1670)$	0.10	$\eta\rho_3(1690)$	<0.01
	$KK_3(1780)$	<0.01		
$1^- \to 1^-1^+$	$b_1(1235)\rho$	0.91	$K_1(1400)K^*$	<0.01
	$a_1(1260)\omega$	0.97	$K_1(1270)K^*$	<0.01
	$\rho f_1(1285)$	0.98	$\rho f_1(1420)$	0.07
	$\rho h_1(1170)$	0.77		
$1^- \to 2^+1^-$	$\rho f_2(1270)$	0.37	$K^*K_2^*(1430)$	<0.01
	$\omega a_2(1320)$	0.05		
$1^- \to 0^-4^+$	$a_4(1970)\pi$	0.31		
$1^- \to 1^-0^+$	$a_0(1450)\omega$	0.27		
Total width		23.88		

V. SUMMARY AND CONCLUSION

In this work, we present the masses and strong decay widths of the higher excited ρ mesons $\rho(5^3S_1)$, $\rho(4^3D_1)$, $\rho(6^3S_1)$, $\rho(5^3D_1)$, $\rho(7^3S_1)$, and $\rho(6^3D_1)$. The deviations between the theoretical masses predicted with MGI and GI models are about 300–500 MeV, which implies that the screening effects are important for the higher excited ρ mesons. We also show some experimental hints for the existences of the higher excited ρ mesons, and one cannot claim these resonances based on the poor measurements at present.

In addition to the masses of the higher exited ρ mesons, the strong decay widths are also calculated, which are $\Gamma_{\rho(5S)} = 143$ MeV, $\Gamma_{\rho(4D)} = 106$ MeV, $\Gamma_{\rho(6S)} = 67$ MeV, $\Gamma_{\rho(5D)} = 59$ MeV, $\Gamma_{\rho(7S)} = 61$ MeV, and $\Gamma_{\rho(6D)} = 24$ MeV, respectively. According to our theoretical predictions, those states are expected to be observed in the final states of 4π, 6π, $\eta\pi\pi$, $\pi K\bar{K}$, $\omega a_2(1320)$. Our theoretical study on their masses and decay properties should be useful to search for these resonances experimentally.

ACKNOWLEDGMENTS

This work is supported by the Natural Science Foundation of Henan under Grant No. 222300420554. It is also supported by the Project of Youth Backbone Teachers of Colleges and Universities of Henan Province (Grant No. 2020GGJS017).

[1] M. Ablikim *et al.* (BESIII Collaboration), Measurement of $e^+e^- \to K^+K^-$ cross section at $\sqrt{s} = 2.00$–3.08 GeV, Phys. Rev. D **99**, 032001 (2019).

[2] M. Ablikim *et al.* (BESIII Collaboration), Observation and study of the decay $J/\psi \to \phi\eta\eta'$, Phys. Rev. D **99**, 112008 (2019).

[3] P. A. Zyla *et al.* (Particle Data Group), Review of particle physics, Prog. Theor. Exp. Phys. **2020**, 083C01 (2020).

[4] B. Aubert *et al.* (*BABAR* Collaboration), Measurements of $e^+e^- \to K^+K^-\eta$, $K^+K^-\pi^0$ and $K^0_S K^\pm\pi^\mp$ cross sections using initial state radiation events, Phys. Rev. D **77**, 092002 (2008).

[5] M. Ablikim *et al.* (BESIII Collaboration), Observation of a resonant structure in $e^+e^- \to \omega\eta$ and another in $e^+e^- \to \omega\pi^0$ at center-of-mass energies between 2.00 and 3.08 GeV, Phys. Lett. B **813**, 136059 (2021).

[6] M. Ablikim *et al.* (BESIII Collaboration), Partial-wave analysis of $J/\psi \to K^+K^-\pi^0$, Phys. Rev. D **100**, 032004 (2019).

[7] J. P. Lees *et al.* (*BABAR* Collaboration), Resonances in e^+e^- annihilation near 2.2 GeV, Phys. Rev. D **101**, 012011 (2020).

[8] J. C. Feng, X. W. Kang, Q. F. Lü, and F. S. Zhang, Possible assignment of excited light $^3S_1$ vector mesons, Phys. Rev. D **104**, 054027 (2021).

[9] L. M. Wang, J. Z. Wang, and X. Liu, Toward $e^+e^- \to \pi^+\pi^-$ annihilation inspired by higher ρ mesonic states around 2.2 GeV, Phys. Rev. D **102**, 034037 (2020).

[10] P. Masjuan, E. Ruiz Arriola, and W. Broniowski, Reply to "Comment on 'Systematics of radial and angular-momentum Regge trajectories of light nonstrange $q\bar{q}$-states' ", Phys. Rev. D **87**, 118502 (2013).

[11] C. Q. Pang, Y. R. Wang, J. F. Hu, T. J. Zhang, and X. Liu, Study of the ω meson family and newly observed ω-like state $X(2240)$, Phys. Rev. D **101**, 074022 (2020).

[12] C. Q. Pang, Excited states of ϕ meson, Phys. Rev. D **99**, 074015 (2019).

[13] C. G. Zhao, G. Y. Wang, G. N. Li, E. Wang, and D. M. Li, $\phi(2170)$ production in the process $\gamma p \to \eta\phi p$, Phys. Rev. D **99**, 114014 (2019).

[14] M. Piotrowska, C. Reisinger, and F. Giacosa, Strong and radiative decays of excited vector mesons and predictions for a new $\phi(1930)$ resonance, Phys. Rev. D **96**, 054033 (2017).

[15] M. K. Volkov, K. Nurlan, and A. A. Pivovarov, Production $\rho(770)$ of meson pairs in the decays $\rho(1450) \to \rho(770)\eta$ and $\tau \to \rho(770)\eta\nu_\tau$ and in the process $e^+e^- \to \rho(770)\eta$ in the extended Nambu–Jona-Lasinio model, JETP Lett. **106**, 771 (2017).

[16] L. Y. Xiao, X. Z. Weng, X. H. Zhong, and S. L. Zhu, A possible explanation of the threshold enhancement in the process $e^+e^- \to \Lambda\bar{\Lambda}$, Chin. Phys. C **43**, 113105 (2019).

[17] K. T. Chao, Y. B. Ding, and D. H. Qin, Possible phenomenological indication for the string Coulomb term and the color screening effects in the quark—anti-quark potential, Commun. Theor. Phys. **18**, 321 (1992).

[18] Y. B. Ding, K. T. Chao, and D. H. Qin, Screened Q anti-Q potential and spectrum of heavy quarkonium, Chin. Phys. Lett. **10**, 460 (1993).

[19] Z. Y. Li, D. M. Li, E. Wang, W. C. Yan, and Q. T. Song, Assignments of the $Y(2040)$, $\rho(1900)$, and $\rho(2150)$ in the quark model, Phys. Rev. D **104**, 034013 (2021).

[20] A. Hasan and D. V. Bugg, Amplitudes for $\bar{p}p \to \pi\pi$ from 0.36 GeV/c to 2.5 GeV/c, Phys. Lett. B **334**, 215 (1994).

[21] A. V. Anisovich, C. A. Baker, C. J. Batty, D. V. Bugg, L. Montanet, V. A. Nikonov, A. V. Sarantsev, V. V. Sarantsev, and B. S. Zou, Combined analysis of meson channels with $I = 1, C = -1$ from 1940 to 2410 MeV, Phys. Lett. B **542**, 8 (2002).

[22] B. Aubert *et al.* (*BABAR* Collaboration), The $e^+e^- \to 3(\pi^+\pi^-), 2(\pi^+\pi^-\pi^0)$ and $K^+K^-2(\pi^+\pi^-)$ cross sections at center-of-mass energies from production threshold to 4.5-GeV measured with initial-state radiation, Phys. Rev. D **73**, 052003 (2006).

[23] B. Aubert *et al.* (*BABAR* Collaboration), The $e^+e^- \to 2(\pi^+\pi^-)\pi^0$, $2(\pi^+\pi^-)\eta$, $K^+K^-\pi^+\pi^-\pi^0$ and $K^+K^-\pi^+\pi^-\eta$ cross sections measured with initial-state radiation, Phys. Rev. D **76**, 092005 (2007); **77**, 119902(E) (2008).

[24] P. Lichard, Common explanation of the behavior of some e^+e^- annihilation processes around $\sqrt{s} = 1.9$ GeV, Phys. Rev. D **98**, 113011 (2018).

[25] L. M. Wang, S. Q. Luo, and X. Liu, Light unflavored vector meson spectroscopy around the mass range of 2.4–3 GeV and possible experimental evidence, Phys. Rev. D **105**, 034011 (2022).

[26] S. Godfrey and N. Isgur, Mesons in a relativized quark model with chromodynamics, Phys. Rev. D **32**, 189 (1985).

[27] C. Q. Pang, J. Z. Wang, X. Liu, and T. Matsuki, A systematic study of mass spectra and strong decay of strange mesons, Eur. Phys. J. C **77**, 861 (2017).

[28] Q. F. Lü and D. M. Li, Understanding the charmed states recently observed by the LHCb and *BABAR* Collaborations in the quark model, Phys. Rev. D **90**, 054024 (2014).

[29] Q. F. Lü, T. T. Pan, Y. Y. Wang, E. Wang, and D. M. Li, Excited bottom and bottom-strange mesons in the quark model, Phys. Rev. D **94**, 074012 (2016).

[30] Q. T. Song, D. Y. Chen, X. Liu, and T. Matsuki, Charmed-strange mesons revisited: mass spectra and strong decays, Phys. Rev. D **91**, 054031 (2015).

[31] X. C. Feng, Wei-Hao, and l. J. Liu, The assignments of the bottom mesons within the screened potential model and $^3P_0$ model, Int. J. Mod. Phys. E **31**, 2250066 (2022).

[32] K. D. Born, E. Laermann, N. Pirch, T. F. Walsh, and P. M. Zerwas, Hadron properties in lattice QCD with dynamical fermions, Phys. Rev. D **40**, 1653 (1989).

[33] Q. T. Song, D. Y. Chen, X. Liu, and T. Matsuki, Higher radial and orbital excitations in the charmed meson family, Phys. Rev. D **92**, 074011 (2015).

[34] J. Z. Wang, D. Y. Chen, X. Liu, and T. Matsuki, Constructing J/ψ family with updated data of charmoniumlike Y states, Phys. Rev. D **99**, 114003 (2019).

[35] J. Z. Wang, Z. F. Sun, X. Liu, and T. Matsuki, Higher bottomonium zoo, Eur. Phys. J. C **78**, 915 (2018).

[36] W. Hao, G. Y. Wang, E. Wang, G. N. Li, and D. M. Li, Canonical interpretation of the $X(4140)$ state within the $^3P_0$ model, Eur. Phys. J. C **80**, 626 (2020).

[37] T. G. Li, Z. Gao, G. Y. Wang, D. M. Li, E. Wang, and J. Zhu, The possible assignments of the scalar $K_0^*(1950)$ and

$K_0^*(2130)$ within the $^3P_0$ model, Phys. Rev. D **106**, 034012 (2022).

[38] Z. Gao, G. Y. Wang, Q. F. Lü, J. Zhu, and G. F. Zhao, Canonical interpretation of the $D_s^0(2590)^+$ resonance, Phys. Rev. D **105**, 074037 (2022).

[39] C. Q. Pang, Y. R. Wang, and C. H. Wang, Prediction for 5^{++} mesons, Phys. Rev. D **99**, 014022 (2019).

[40] T. T. Pan, Q. F. Lü, E. Wang, and D. M. Li, Strong decays of the $X(2500)$ newly observed by the BESIII Collaboration, Phys. Rev. D **94**, 054030 (2016).

[41] G. Y. Wang, S. C. Xue, G. N. Li, E. Wang, and D. M. Li, Strong decays of the higher isovector scalar mesons, Phys. Rev. D **97**, 034030 (2018).

[42] S. C. Xue, G. Y. Wang, G. N. Li, E. Wang, and D. M. Li, The possible members of the 5^1S_0 meson nonet, Eur. Phys. J. C **78**, 479 (2018).

[43] L. Micu, Decay rates of meson resonances in a quark model, Nucl. Phys. **B10**, 521 (1969).

[44] A. Le Yaouanc, L. Oliver, O. Pene, and J. C. Raynal, Naive quark pair creation model of strong interaction vertices, Phys. Rev. D **8**, 2223 (1973).

[45] A. Le Yaouanc, L. Oliver, O. Pene, and J. C. Raynal, Naive quark pair creation model and baryon decays, Phys. Rev. D **9**, 1415 (1974).

[46] H. G. Blundell, Meson properties in the quark model: A look at some outstanding problems, arXiv:hep-ph/9608473.

[47] C. Hayne and N. Isgur, Beyond the wave function at the origin: Some momentum dependent effects in the nonrelativistic quark model, Phys. Rev. D **25**, 1944 (1982).

[48] M. Jacob and G. C. Wick, On the general theory of collisions for particles with spin, Ann. Phys. (N.Y.) **7**, 404 (1959).

[49] A. V. Anisovich, V. V. Anisovich, and A. V. Sarantsev, Systematics of $q\bar{q}$ states in the (n, M^2) and (J, M^2) planes, Phys. Rev. D **62**, 051502 (2000).

[50] H. Y. Cheng, Revisiting axial-vector meson mixing, Phys. Lett. B **707**, 116 (2012).